

Numerical Study of Effects of Synclinal Basement Topography on Ground Motion Characteristics



J.P. Narayan and V. Kumar

*Department of Earthquake Engineering,
Indian Institute of Technology Roorkee, Roorkee -247 667, INDIA
jaypnfeq@iitr.ernet.in; vinaytomar23@gmail.com*

SUMMARY:

The effects of radius of curvature, focal length and depth of synclinal basement topography (SBT) on ground motion characteristics in both the quantitative and qualitative manners are documented in this paper. Seismic responses of various unbounded SBT models were computed using a 2D fourth-order spatial accurate SH-wave finite-difference (FD) algorithm. In order to accurately quantify the SBT effects on the spectral amplification of ground motion, a frequency dependent damping in time-domain FD simulation is implemented based on rheology of generalised Maxwell body, widely known as GMB-EK rheological model. The computed seismic responses on the vertical array along the focal length as well as snapshots at various times revealed that the amplification pattern caused by SBT very much depends on radius of curvature, focal length, depth of SBT and the rheology of the sediment overlying the basement. The spectral amplification caused by SBT is computed just by taking the spectral ratio of responses with and without SBT in the model in order to exclude the effects of impedance contrast at the sediment basement interface. A frequency dependent amplification of ground motion is inferred. Results of this study depict that consideration of SBT effect is as much important as that of surface hills/ridges during seismic hazard assessment.

Keywords: Basement topography effects, focusing and defocusing effects, finite difference simulation.

1. INTRODUCTION

Sometimes very peculiar damage pattern is observed, which cannot be explained based on the soil amplification or soil resonance effects as was observed in Santa Monica, Los Angeles basin during Northridge earthquake of 1994 (Alex and Olsen, 1998; Davis et al., 2000) and consistently in Seattle, Washington during earthquakes of 1949, 1965 and 2001 (Booth et al., 2004; Stephenson et al., 2006). Alex and Olsen (1998) simulated finite-difference (FD) responses of Santa Monica region and inferred that deep basement focusing can only account around 50% amplification of ground motion observed in Santa Monica. Davis et al. (2000) carried out inversion of aftershock earthquake records using SH-wave FD simulation and inferred that the damage in Santa Monica occurred due to focusing caused by the presence of several underground acoustic lenses at depths of around 3 km in Los Angeles basin.

Another well known and accepted example of basement focusing effects on the ground motion characteristics is the consistent anomalous damage to unreinforced brick chimneys in west Seattle, Washington during 1949 Olympia earthquake of magnitude 7.1, 1965 Tacoma earthquake of magnitude 6.5 and 2001 Nisqually earthquake of magnitude 6.8 (Booth et al., 2004; Stephenson et al., 2006). Frankel et al. (2002) reported a nearly 3-times amplification of horizontal acceleration at 1.0Hz in highly chimney damage area as compared to the nearby region where there was less damage to the same during 2001 Nisqually earthquake. Stephenson et al. (2006) simulated the shallow seismic focusing effects and resolved the ground motion mystery in west Seattle which caused anomalous consistent damage to chimneys during earthquakes of 1949, 1965 and 2001. The effects of synclinal

basement topography (SBT), its curvature, depth and sediment rheology on ground motion characteristics are studied in details. Seismic responses of an unbounded SBT model on a vertical array along the focal length are simulated for different sediment rheology and curvature of SBT.

2. SALIENT FEATURES OF THE FINITE- DIFFERENCE ALGORITHM

Realistic quantification of local site effects on the ground motion characteristics requires an efficient numerical method (Narayan, 2011; Narayan and Kumar, 2008; Kumar and Narayan, 2008), particularly the incorporation of realistic damping in time domain simulations. Day and Minster (1984) made first attempt to incorporate viscoelastic damping in time-domain FD simulations. Just after this pioneer work, two independent approaches were developed based on rheological property and behavior of real earth material - namely rheology of generalized Maxwell body (GMB-EK model) (Emmerich and Korn, 1987) and rheology of generalized Zener body (GZB model) (Carcione et al., 1988). However, Moczo and Kristek (2005) demonstrated that both the GMB-EK and GZB rheological models are equivalent. The program used in this simulation is developed By Narayan and Kumar (2012) which is based on the (2,4) staggered grid finite-difference approximation of viscoelastodynamic SH-wave equations using GMB-EK rheological model and material independent anelastic function (Emmerich and Korn, 1987; Kristek and Moczo, 2003). Fig. 1. shows the staggering technique, where particle velocity (V) and the density (ρ) are defined at the nodes and the shear stresses (σ_{xy} and σ_{zy}), modified unrelaxed modulus of rigidity ($\bar{\mu}_u$), anelastic coefficients (\bar{Y}_l) and anelastic functions (χ) are defined at the midway between the two adjacent grid points. The input parameters namely unrelaxed modulus and anelastic coefficients have been obtained using phase velocity of S-wave (V_{S,ω_r}) and quality factor at reference frequency (ω_r) (Moczo et al., 1997). The material independent anelastic function, modified unrelaxed modulus of rigidity and modified anelastic coefficients have been computed at four relaxation frequencies ($\omega_l = 4$), the details are given in Moczo et al. (2005). The effective values of the unrelaxed modulus of rigidity are obtained using harmonic mean.

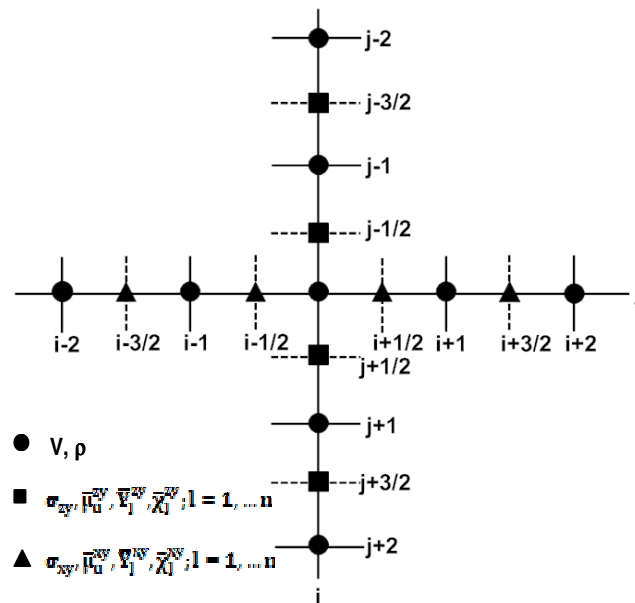


Figure 1. Staggering technique for SH-wave modeling with fourth order spatial accuracy. Particle velocity and density are defined at grid nodes and shear stress components and relaxed modulus of rigidity, anelastic coefficients and anelastic functions are defined at the midway between two adjacent grid points.

The response of an unbounded homogeneous viscoelastic medium at different distances on a vertical array is used to show the accuracy of use FD algorithm. The S-wave velocity and quality factor at reference frequency ($F_r=1$ Hz), density and unrelaxed modulus of rigidity are given in table 1. Four relaxation frequencies were taken as 0.02 Hz, 0.2 Hz, 2.0 Hz and 20 Hz. A Ricker wavelet with 4.0 Hz dominant frequency with a considerable spectral amplitude in frequency range of 0.25 Hz to 10.0 Hz was used as an excitation function for generating a horizontal line source. The spectral amplitude ratios A_x/A_0 were computed for different distance travelled (x). The trace recorded nearest to the line source was used as a reference trace. The spectral amplitude ratios for the same distance travelled were also computed using the phase velocity and quality factors obtained using Futterman's relation and GMB-EK model. Figure 2 shows a comparison of numerically computed spectral amplitude ratio A_x/A_0 for distance travelled as 1500 m, 3000m, 4500m and 6000m and the same computed using phase velocity and quality factors obtained using Futterman's relationship and GMB-EK model. The excellent matching of analytically and numerically computed spectral amplitude ratios validates the accuracy of procedure of implementation of realistic damping in the developed time domain SH-wave finite-difference algorithm.

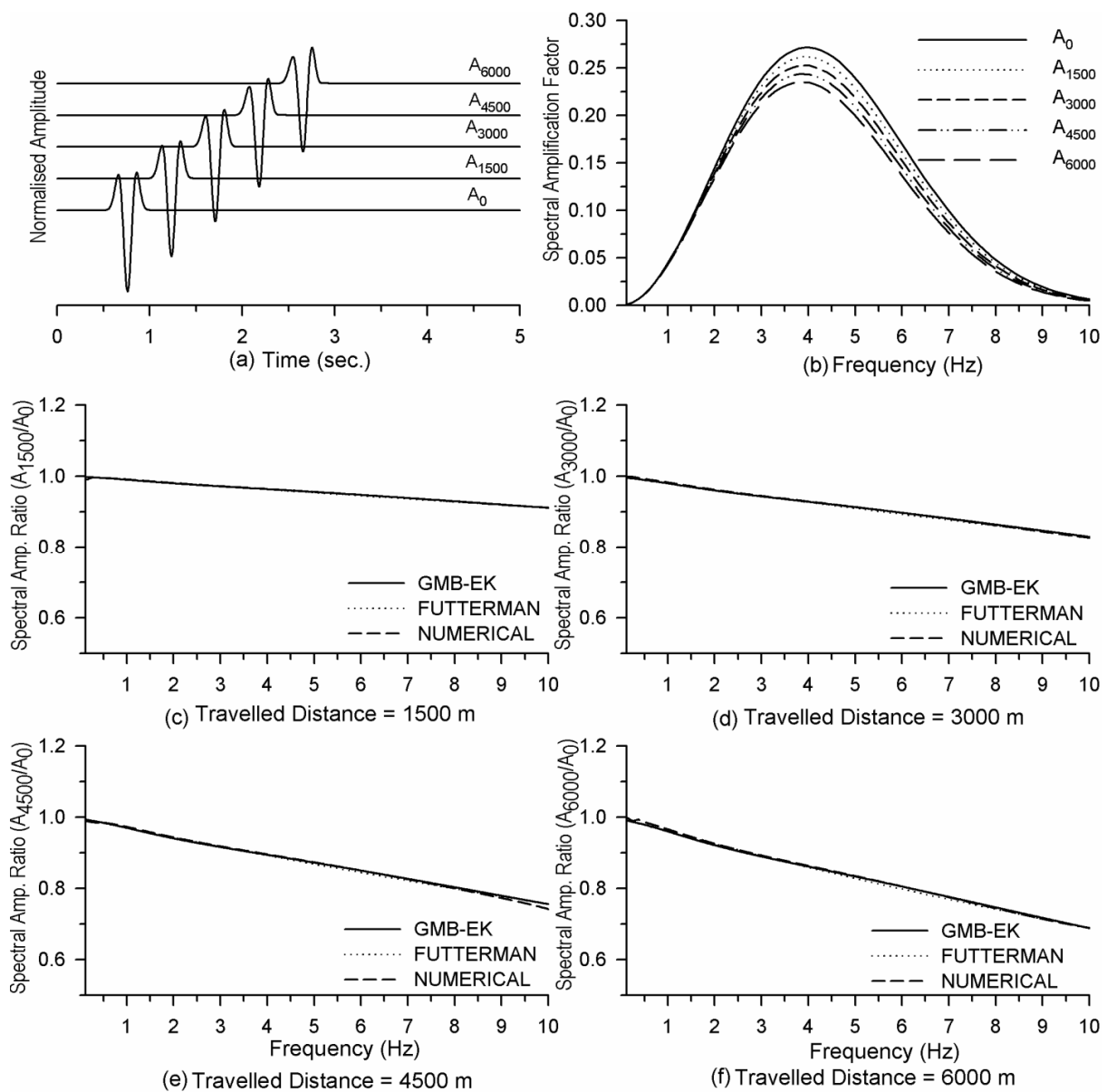


Figure 2. Spectral amplitude ratio for various distance travelled.

3. EFFECTS OF SYNCLINAL BASEMENT TOPOGRAPHY

In order to study the effects of synclinal basement topography on the ground motion characteristics, an unbounded circular SBT-model consisting of elastic sedimentary deposit is considered. Figure 3 shows the half-circular SBT-model with radius 3000 m. The S-wave velocity and density of sedimentary deposit were taken as 1750 m/s and 2.0 gm/cc and that in basement rock were 3200 m/s and 2.8 gm/cc. A plane SH-wave front was generated at a depth of 1000 m below the tip of SBT. Time step was taken as 0.002s. Seismic responses were computed at 15 equidistant (500 m apart) receiver points on a vertical array extending from 450 m below the tip of SBT to 6550 m above the same. Seismic responses without SBT were also computed taking the same model parameters and the source receiver configuration but keeping the position of horizontal interface between sedimentary deposit and the basement rock at the tip of the SBT.

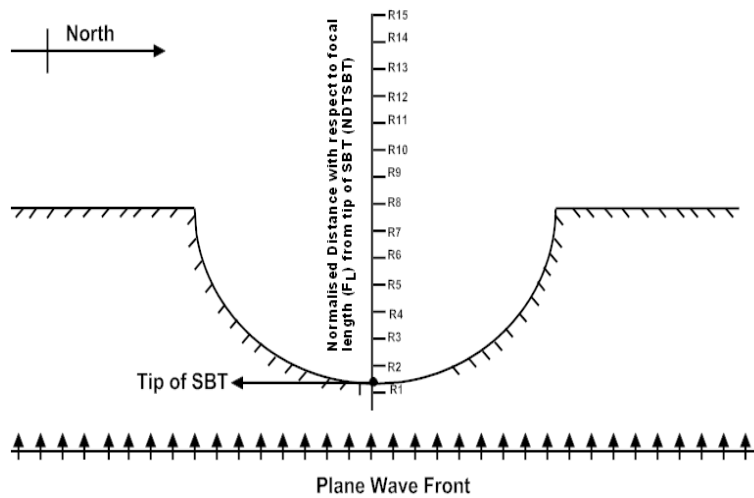


Figure 3. SBT-model with a vertical array passing along the focal length of SBT.

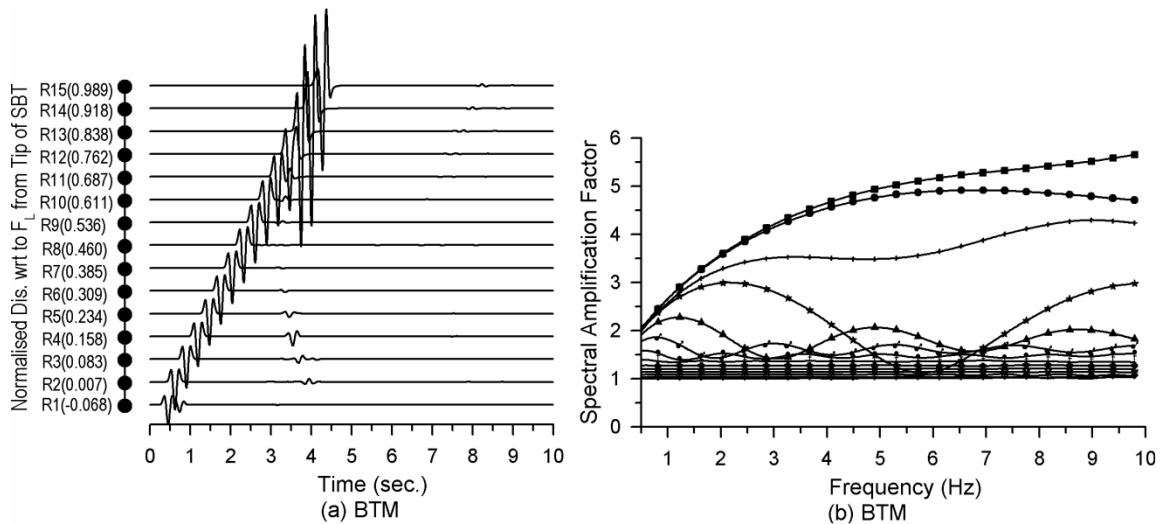


Figure 4 a&b. Seismic responses and spectral amplifications at different NDTSBT positions.

Figure 4a shows the simulated elastic seismic response on a vertical array. The normalised distance of receiver points from the tip of SBT with respect to the focal length (F_L) of SBT are given in the brackets. An analysis of figure 4 depicts that there is tremendous increase of amplitude of transmitted SH-wave in basin towards the focus of the SBT due to SBT-focusing effect. Diffracted waves from the top corners of the SBT are very clearly visible on receivers R2-R10. The amplitude of diffracted

waves was highly variable due to divergence, damping and the interference effects. Diffracted waves are merged with the SH-wave on receivers R11-R15. A decrease of amplitude of SH-wave at R15 very near the focus can be inferred. Maximum amplitude of SH-wave was obtained at receiver R14 at a distance of 6050 m from the tip of SBT, instead of at the focus. The receiver R1 located in basement depicts both the up-going SH-wave and the reflected SH-wave from the SBT.

In order to further demonstrate the SBT-focusing effects and development of diffractions from the corners of SBT, snapshots were computed in a rectangular area at different times. Snapshots were computed in an area extending from 730 m down to 6750 m up of the tip of SBT and 5000 m south to 5000 m north of tip of SBT. The snapshot at time 0.2 second, shown in figure 5a, depicts the just entering linear SH-wave front in the considered rectangular area. Figure 5b shows the SH-wave entered into the synclinal part of SBT and touching the horizontal flanks of the SBT. The reflected SH-wave from the curved part of SBT can also be inferred in this snapshot at time 1.0 second.

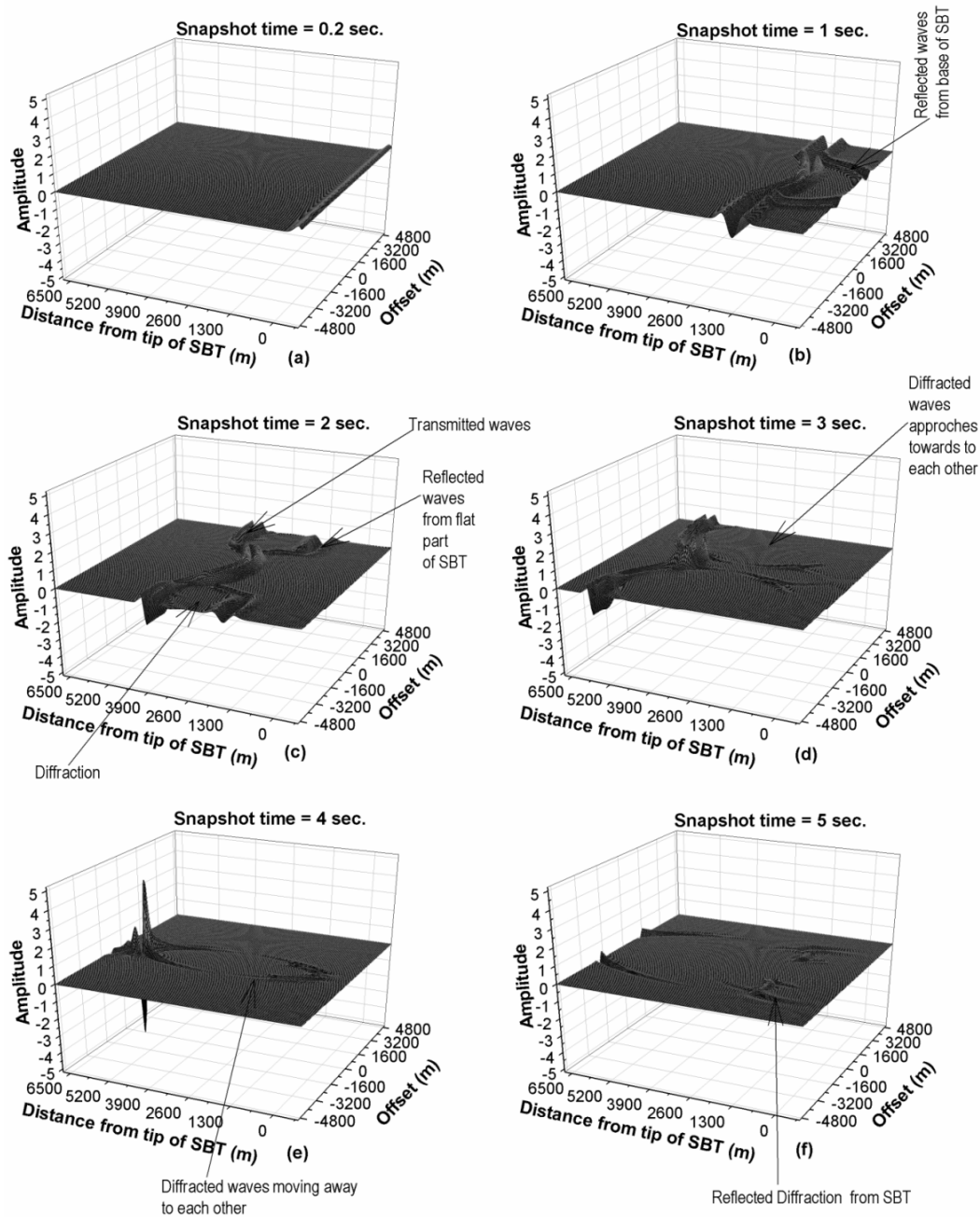


Figure 5. Snapshots in a rectangular area at different times.

The transmitted SH-wave in sediment and their focusing can be inferred in snapshot at time 2.0 second (Fig. 5c). The reflected waves from the horizontal part of SBT and diffracted SH-waves from the corners of SBT can also be inferred in this snapshot. The snapshots at times 3.0 and 4.0 seconds clearly depict the increase of amplitude of transmitted SH-wave towards the focus. The diffracted waves from the corners of the SBT and their amplitude variations are more clearly visible in these snapshots. Snapshot at time 5.0 second (Fig. 5f) reveals only diffracted waves and the reflected diffracted waves from the synclinal part of SBT.

To assess the SBT-focusing effect on the ground motion characteristics quantitatively, spectral amplitude amplification of SH-wave in each trace recorded above the SBT is computed with respect to the trace recorded just above the horizontal basement at the same distance as that of second receiver point in case SBT models. The spectral amplitude amplifications at different locations is shown in figure 4b. Diffracted waves have been removed purposely from the traces where it was possible during the computation of spectra. Analysis of this figure depicts an increase of spectral amplification with increase of NDTSBT value. It can also be inferred that spectral amplification is increasing with the increase of frequency. Further, the rate of increase of spectral amplification with frequency is increasing with the increase of NDTSBT value. But, spectral amplification is very much affected by the presence of diffracted waves in the traces where it was not possible to remove. Maximum effect of diffraction can be seen in record at NDTSBT value equal to 0.76. The largest spectral amplification was obtained of the order of 5.66 for frequency 10 Hz at NDTSBT value equal to 0.91.

3.1. Effect of Rheology of Sediment

In order to study the effects of rheology of sediment on the SBT-focusing effect, seismic responses of a SBT model with radius 3000 m and different rheological models for sediment (BTVM1-BTVM4) were computed, as shown in figure 6. The rheological parameters namely velocity and quality factor at reference frequency, density and unrelaxed modulus of rigidity for different type of sediment above the basement are given in Table 1. The rheological parameters for basement namely velocity and quality factor at reference frequency, density and unrelaxed modulus of rigidity are 3200 m/s, 320, 2.8 g/cc and 28.93 GPa, respectively. Analysis of figure 6 reveals an increase of amplitude of SH- wave towards focus as well as the impedance contrast at the interface of sediment and basement. The effect of focal length is very much clear since number of receiver points on which there is decrease of SH-wave amplitude because of defocusing is increase with the decrease of focal length.

Table 1. Rheological parameters for sediments in case of different basement topography models (BTVM1-BTVM4).

Model Parameters	BTVM1	BTVM2	BTVM3	BTVM4
Velocity at F_R (m/sec.)	1750	1500	1250	1000
Density (kg/m^3)	2200	2050	1950	1800
Quality Factor at F_R	175	175	175	175
Unrelaxed Rigidity (GPA)	6.851	4.690	3.098	1.830

The spectral amplification computed at different NDTSBT positions is given in figure 7. An increase of spectral amplification with the decrease of sediment velocity can be inferred only at NDTSBT positions very near the focus. This may be due to the effects of diffracted waves. Further, higher frequencies are more damped as compared to the lower frequencies; even higher frequencies were more amplified due to the SBT-focusing as was inferred from the analysis of elastic SBT-model (BTM). For example, the spectral amplification was proportional to frequency up to 4.69 Hz, 6.02 Hz, 6.83 Hz and 3.46 Hz in case of BTVM1-BTVM4 models at NDTSBT equal to 0.83, 0.89, 0.92, and 0.92, respectively. The upper frequency up to which spectral amplification is proportional to frequency is decreasing with the decrease of NDTSBT value. But, these inferred effects were highly affected by the presence of diffracted waves.

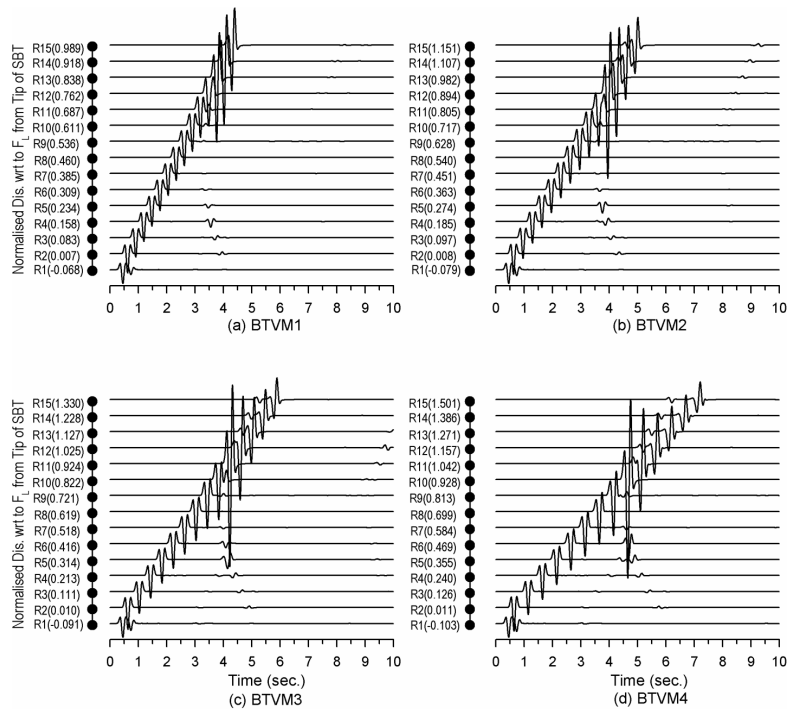


Figure 6. Seismic responses for different BTVM1-BTVM4 models.

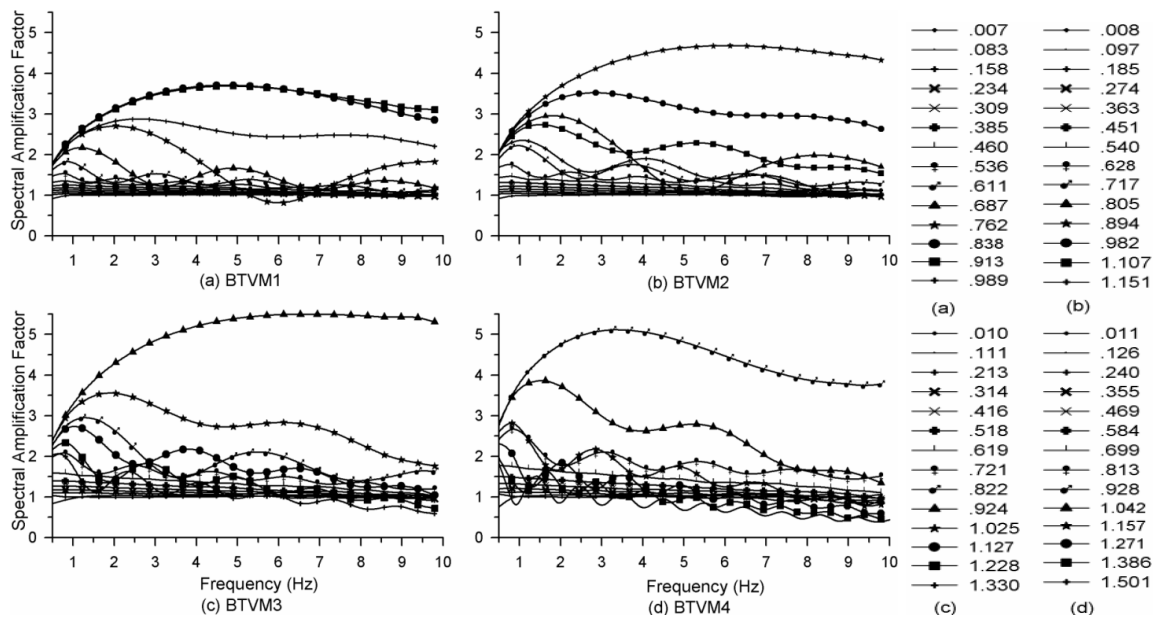


Figure 7. Spectral amplifications at different NDTSBT positions for BTVM1-BTVM4 models.

The computed amplitude amplification in time domain and average spectral amplification at different NDTSBT positions is shown in figure 8. There is a linear increase of both the amplitude amplification and average spectral amplification with the increase of NDTSBT value up to 0.75 thereafter increase of average spectral amplification with NDTSBT value is very large. The average spectral amplification for different IC (BTVM models) is almost same up to NDTSBT value equal to 0.75, thereafter it seems to be different in different models. It appears that this dissimilarity is arising because of very large amplification near the focus and different NDTSBT values available in different models.

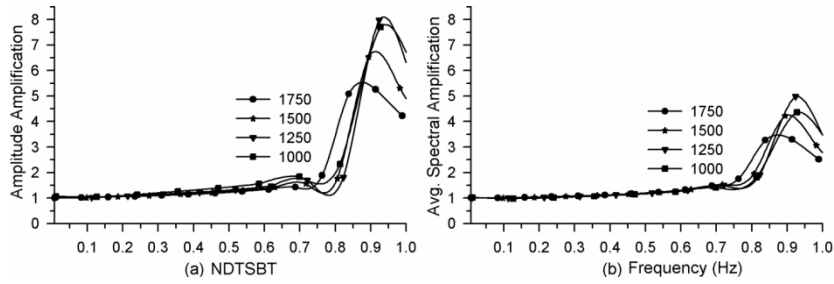


Figure 8 a&b. Amplitude amplification in time domain and average spectral amplification factors at different NDTSBT values for different impedance contrast at the interface of sediment and basement.

3.2. Effects of radius of curvature

To study the effects of radius of curvature of SBT on the ground motion characteristics, different basement models BTRM1, BTRM2, BTRM3 and BTRM4 with radius of curvature as 3000 m, 3250 m, 3500 m, and 3750 m were considered. The rheological parameters namely velocity and quality factor at reference frequency, density and unrelaxed modulus of rigidity for sediment were taken as 1000 m/s, 100, 1800 kg/m³ and 1.853 GPa, respectively and that for basement were taken 3200 m/s, 320, 2.8 g/cc and 28.93 GPa, respectively. The spectral amplifications at different NDTSBT positions corresponding to different models (BTRM1-BTRM4) are shown in figure 9. Analysis of this figure depicts an increase of spectral amplification with increase of NDTSBT value. It can also be inferred that spectral amplification is increasing with the increase of frequency but up to certain frequency.

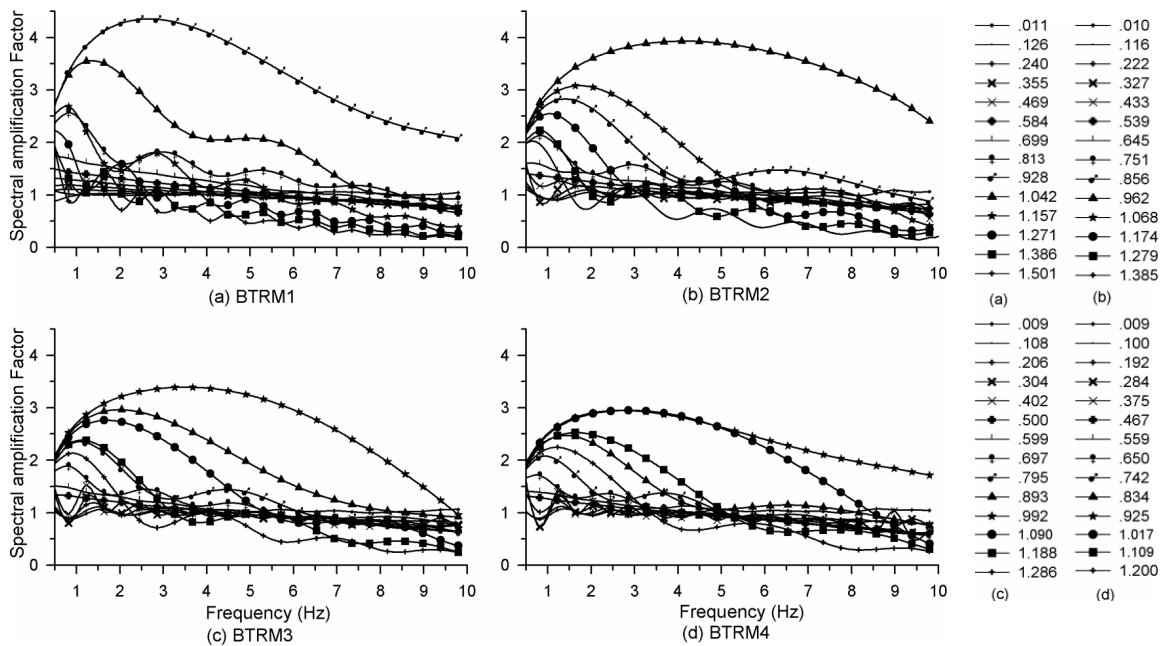


Figure 9. Spectral amplifications at different NDTSBT positions for BTRM1-BTRM4 models.

The computed amplitude amplification in time domain at different NDTSBT positions is shown in figure 10a. There is an increase of amplitude amplification in time domain with the increase of NDTSBT value. The average spectral amplifications at different NDTSBT positions (Fig. 10b) depict an increase of average spectral amplification with the increase of NDTSBT value and minor decrease with the increase of radius of curvature. The minor decrease of average spectral amplification may be due to the larger distance travelled in case of larger radius of curvature. The trend of decrease of average spectral amplification is inferred up to NDTSBT value equal to 0.75 only since thereafter increase of average spectral amplification with NDTSBT value is very large and different value of

NDTSBT constrained by the receiver positions. Analysis of figure 10 depicts that amplitude amplification in time domain is very much similar to the average spectral amplification up to a distance of NDTSBT value equal to 0.75, thereafter amplitude amplification in time domain is larger than the average spectral amplification. It can be concluded that basement focusing effects at different NDTSBT value is same for different radius of curvature with a fixed aperture length. But, the observed trend of decrease with the increase of radius of curvature may be due to effect of sediment damping because of larger distance travelled.

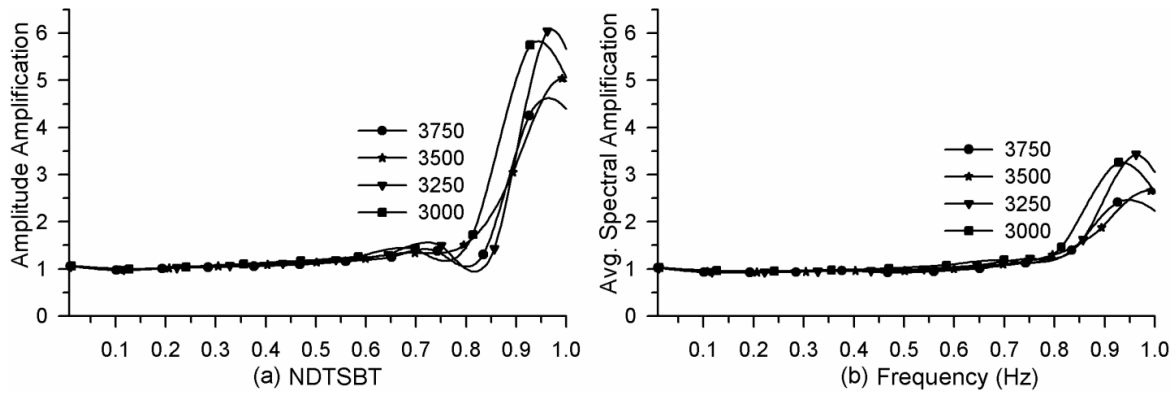


Figure 10 a&b. Amplitude amplification in time domain and average spectral amplification factors at different NDTSBT values for different radius of curvatures.

4. DISCUSSION AND CONCLUSIONS

The accuracy of used FD algorithm is verified by matching of spatial spectral amplitude decrease with the distance travelled by comparing the same computed analytically using phase velocity and quality factor based on GMB-EK rheology (Futterman, 1962; Emmerich and Korn, 1987; Kristek and Mozco, 2003; Mozco and Kristek, 2005). The snapshots along with the elastic simulated responses of SBT model revealed a SBT-focusing effects and the generation of diffracted waves from the top corners of the SBT. The maximum SBT focusing was inferred at a distance of around 0.91 times the focal length of SBT, instead of at the focus. A good similarity in increase of amplitude amplification and average spectral amplification towards the SBT-focus was observed up to a distance of around 0.75 times the focal length of SBT. Thereafter, amplitude amplification was larger than that of average spectral amplification.

An increase of spectral amplification was inferred with the increase of frequency and distance from the tip of SBT towards the focus. Further, an increase of rate of spectral amplification with frequency was also inferred with the increase of distance from the tip of SBT. This effect was also reported by Davis et al. (2000) based on the analytical solutions. Maximum spectral amplification in case of viscoelastic rheology was obtained as 3.7, 4.6, 5.4 and 5.1 in BTVM1-BTVM4 models, respectively. Frankel et al. (2002) reported amplification factor of around 3.0 for horizontal acceleration at 1.0 Hz in West Seattle area where chimney suffered more damage during 2001 Nisqually earthquake. The range of average spectral amplification obtained up to at a distance of around 0.76 times the focal length very much corroborates with the finding of Alex and Olsen (1998), who reported that deep basement focusing can account only around 50% amplification of ground motion observed in Santa Monica region. Based on simulated results, it can be concluded that the exclusive basement focusing effects at different NDTSBT values is more or less same for different radius of curvature with a fixed aperture length and impedance contrast at the interface of sediment and basement. But, it is highly affected by the rheology of the sediment and the diffractions caused by the top corners of SBT.

ACKNOWLEDGEMENT

The first is grateful to the Ministry of Earth Sciences (MoES), New Delhi and Council of Scientific and Industrial Research (CSIR), New Delhi for financial assistance through Grant Numbers MES-484-EQD and CSR-569-EQD, respectively.

REFERENCES

- Alex, C. M., and Olsen, K. B. (1998), Lens-effect in Santa Monica?, *Geophysical Research Letter* **25**, 3441–3444.
- Booth, D. B., Wells, R. E. and Givler, R. W. (2004), Chimney damage in the greater Seattle area from the Nisqually earthquake of 28 February 2001, *Bulletin of the Seismological Society of America* **94**, 1143–1158.
- Carcione, J. M., Kosloff, D., and Kosloff R., (1988). Wave propagation simulation in a linear viscoacoustic medium. *Geophysical Journal* **93**, 393-407.
- Davis, P.M., Justin, L., Rubinstein, K. H., Liu, S. S., and Knopoff., G. L. (2000). Northridge earthquake damage caused by geologic focusing of seismic waves, *Science*, 289, 1746-1750.
- Day, S. M., and Minster, J. B. (1984). Numerical simulation of wave fields using a Padé approximant method. *Geophysical Journal of the Royal Astronomical Society* **78**, 105-118.
- Emmerich, H., and Korn, M. (1987). Incorporation of attenuation into time-domain computations of seismic wave fields. *Geophysics* **52**, 1252-1264.
- Frankel, A. D., Carver, D. L., and Williams, R. A. (2002). Nonlinear and linear site response and basin effects in Seattle for the M6.8 Nisqually, Washington, earthquake, *Bulletin of the Seismological Society of America* **92**, 2090– 2109.
- Futterman, W.I. (1962). Dispersive body waves, *Journal of Geophysical Research* **67**, 5279-5291.
- Kristek, J., and Moczo, P. (2003). Seismic wave propagation in viscoelastic media with material discontinuities- a 3 D 4th order staggered grid finite difference modeling. *Bulletin of the Seismological Society of America* **93**, 2273-2280.
- Kumar, S., and Narayan, J.P. (2008). Importance of quantification of local site effects based on wave propagation in seismic microzonation, *Journal of Earth Science System* **117** (S2), 731-748.
- Moczo, P., Bystricky, E., Kristek, J., Carcione, J.M. and Bouchon, M. (1997). Hybrid modelling of P-SV seismic motion at inhomogeneous viscoelastic topographic structures, *Bulletin of the Seismological Society of America* **87**, 1305-1323.
- Moczo, P., and Kristek, J. (2005). On the rheological models used for time-domain methods of seismic wave propagation. *Geophysical Research Letter* **32**, L01306, doi: 10.1029/2004GL021598.
- Narayan, J.P., and Kumar, S. (2008). A 4th order accurate SH-wave staggered grid finite-difference algorithm with variable grid size and VGR-stress imaging technique, *Pure and Applied Geophysics* **165**, 271-294.
- Narayan, J.P. (2011). Effects of P-wave and S-wave impedance contrast on the characteristics of basin transduced Rayleigh waves, *Pure and Applied Geophysics* (DOI : 10.1007/s00024-011-0338-7).
- Narayan, J.P., and Kumar, V. (2012). SH-wave time domain finite-difference algorithm with realistic damping and a combined study of effects of sediment rheology and basement focusing. Communicated
- Stephenson, W. J., Frankel, A. D., Odum, J. K., Williams, R. A., and Pratt, T. L. (2006). Toward resolving an earthquake ground motion mystery in west Seattle, Washington State: Shallow seismic focusing may cause anomalous chimney damage, *Geophysical Research Letter* **33**, L06316, doi:10.1029/2005GL025037.